Convolutional Coded Dual Header Pulse Interval Modulation for Line of Sight Photonic Wireless Links

Z. Ghassemlooy and S. Rajbhandari

Optical Communications Research Group,

NCRLab, School of Computing, Engineering & Information Sciences,

Northumbria University, Ellison Building, Newcastle upon Tyne, NE1 8ST, UK

Fary.ghassemlooy@unn.ac.uk

Abstract

The paper presents the analysis and simulation for convolutional coded dual header pulse interval modulation (CC-DH-PIM) scheme using a rate ½ convolutional code with the constraint length of 3. Decoding is implemented using the Viterbi algorithm with a hard decision. Mathematical analysis for the slot error rate upper bounds is presented and results are compared with the simulated data for a number of different modulation techniques. We show that the coded DH-PIM outperforms the pulse position modulation (PPM) scheme and offers > 4 dB code gain at the slot error rate (SER) of 10^{-4} compared to the standard DH-PIM. Results presented show that the CC-DH-PIM with a higher constraint length of 7 offers a code gain of 2 dB at slot error rate of 10^{-5} compared to the CC-DH-PIM with a constraint length of 3. However, in CC-DH-PIM the improvement in the error performance is achieved at the cost of reduced transmission throughput compared to the standard DH-PIM.

1. INTRODUCTION

Photonic wireless, also known as optical wireless (OW) and infrared, communication systems have been around for some time and their applications in both indoor and outdoor environments have been investigated by many researchers [1-6]. The outdoor systems are more mature and widely used compared to the indoor systems, offering unlicensed bandwidth orders of magnitude higher than the radio frequency (RF) based schemes. In indoor applications the potential of wavelength reuse within the same/different location is considerably higher than the RF systems. In fact in direct line-of-sight (LOS) photonic cellular systems a single wavelength could be employed to cover a large or small area, which is not possible in RF based cellular systems [7-9]. However, as with all communication systems there are limitations imposed by the channel characteristics (loss, multipath dispersion in non-LOS) [2, 10], interference due to the ambient light sources [11] and power restrictions due to the eye safety [6] that need investigating. Selecting a suitable modulation scheme may overcome some of the above limitations. However, no single modulation technique will offer both power and bandwidth efficiencies and system performance at a low cost and with the reduced complexity. In applications where there is a high demand for a bandwidth efficiency and a high throughput, power efficient modulation schemes may not be the best choice and vice versa. For indoor and outdoor point-to-point links power efficient modulation scheme would be more advantageous than bandwidth efficient schemes, whereas for indoor diffuse (non-LOS) links bandwidth efficient modulation schemes would be preferable because of multipath propagation and large-area photodiodes. In fact the 3 dB bandwidth of a channel can be less than 30.4 MHz, limiting the unequalized bit rate to few Mbps [2, 12]. Different modulation techniques have been suggested and investigated for a number of applications; among them are on-off keying (OOK), PPM [13], differential PPM (DPPM) [14], digital pulse interval modulation (DPIM) [15], DH-PIM [16] and differential amplitude pulse-position modulation (DAPPM) [17]. OOK is the most basic and widely

investigated, offering a high bandwidth efficiency at the cost of a low power efficiency. In contrast to OOK, PPM is the most power efficient scheme but requires a large bandwidth. PPM is an isochronous modulation scheme, thus requiring both slot and symbol synchronisations. DPIM, DH-PIM and DAPPM are anisochronous modulation schemes offering built-in symbol synchronisation capabilities and improvement in bandwidth and power efficiencies compared to the PPM and OOK, respectively. In terms of transmission capacity and bandwidth, the DH-PIM offers the best choice compared to the PPM and DPIM at the cost of a more complex symbol header structure and higher power requirement for a given bit error rate (BER) performance [16]. DAPPM is a combination of DPPM and pulse amplitude modulation (PAM), offering advantages over PPM, DPPM and DH-PIM in terms of bandwidth requirements, transmission capacity, and the peak-to-average power ratio [17].

In [16] the detailed analysis of a standard un-coded DH-PIM scheme has been reported. In this paper, we introduce the CC-DH-PIM scheme and carry out full theoretical analysis supported by computer simulations to demonstrate that the error performance can be significantly improved compared to the un-coded DH-PIM. We propose a transfer function for the coded DH-PIM, and apply the 'hard' decision Viterbi algorithm to decode the coded sequence. We show that for the SER lower than 10^{-6} the upper bound for the CC-DH-PIM and the general error bound for the convolutional coded modulation scheme almost overlaps. We illustrate that a code gain of > 4 dB is achievable when compared to the standard DH-PIM scheme. The rest of the paper is organised as follows. A CC-DH-PIM system description is presented in Section 2, whereas the analysis for convolutional encoding with the 'hard' decision Viterbi decoding is given in the next section. The theoretical and simulation results for the error performance for CC-DH-PIM, DH-PIM and PPM are given in Section 4. Finally the concluding remarks are given in Section 5.

2. System Description

A system block diagram of the CC-DH-PIM scheme is given in Fig. 1. An M-bit OOK input sequence $m = \{m_1, m_2 \ldots m_M\}$ where $m_i \in (0,1)$ and $M > 1$, an integer is first converted into DH-PIM symbol format $\boldsymbol{X}$ before being applied to the convolutional encoder. The coded DH-PIM symbol $\boldsymbol{Xc}$ is passed through a transmitter filter $p(t)$ with a unit-amplitude impulse response of one slot duration T_s. The output of the transmitter filter $x(t)$ is then applied to a standard optical transmitter (LED or laser diode). In an ideal non-dispersive channel $h(t)$, additive white Gaussian noise (AWGN) $n(t)$ due to the dominant thermal noise is added to the signal before being detected by a photodetector at the receiver. The photocurrent generated due to the ambient light sources can be reduced by means of optical band pass filter and high pass filtering in the receiver. Under the steady state conditions the variation in the photocurrent due to the ambient light sources has no influence, and therefore here a simple channel model has been adopted in this paper. The output of the optical receiver $y(t)$ is applied to a matched filter, followed by a sampler (sampling at the slot rate $f_s = 1/T_s$) and a threshold detector to regenerate the coded DH-PIM sequence $\hat{X}_C$. A 'hard' decision Viterbi decoder is used to recover the original non coded DH-PIM symbol sequence $\hat{X}$. Finally, a DH-PIM demodulator reproduces the original data stream $\hat{m}$. The estimated DH-PIM $\hat{X}$ is compared with the original DH-PIM sequence X to determine the SER.

2.1 DH-PIM

The n^{th} symbol $\boldsymbol{X_n}(h_n,d_n)$ of a DH-PIM sequence is composed of a header h_n, initiating the start of a symbol, and a number of empty information slots d_n. Depending on the most significant bit (MSB) of $\boldsymbol{m}$, one of two possible symbol headers of equal duration $T_h = (\alpha + 1)T_s$, where $\alpha > 0$ is an integer, could be considered; H_0 and H_1 for MSB of "0" and "1", respectively, see Fig. 2. The

value of $d_n \in \{0,1,\ldots,2^{M-1}-1\}$ is simply the decimal value of $\boldsymbol{m}$ or its 1's complement when a symbol starts with H_0 and with H_1, respectively [16]. Figure 2 shows DH-PIM symbol mapping. A guard slot $T_g \in \{(0.5\alpha + 1)\ T_s,\ T_s\}$ corresponding to $h_n \in \{H_0,H_1\}$ is used to represent for $m = 0$. The header pulses have the dual functions of symbol initiation and built-in symbol synchronisation. DH-PIM average duty cycle is $1/\overline{L}$, where $\overline{L} = (2^{M-1} + 2\alpha + 1)/2$ and has a peak-to-average power ratio of $\overline{L}$. DH-PIM average symbol length $\overline{L}$ can be reduced by a proper selection of α, thus offering improved transmission throughput and bandwidth requirements compared to the DPIM, DPPIM and PPM schemes.

For OW systems a baseband additive white Gaussian noise (AWGN) channel model the instantaneous received signal is given as:

$$y(t) = \int_{-\infty}^{\infty} x(\tau)h(t-\tau)d\tau + n(t), \tag{1}$$

where $h(t)$ and $n(t)$ are the channel response and AWGN, respectively. $x(t)$ is the instantaneous transmitted signal which must satisfy $x(t) \geq 0$ and $\overline{x(t)} = \bar{P}$, where $\bar{P}$ the average received optical power. A DH-PIM signal with an average symbol duration $\bar{T}$ satisfying this condition is given as:

$$x(t) = \overline{L}\overline{P}\sum_{M=0}^{\overline{L}-1} X_M\, p(t - \frac{M\overline{T}}{\overline{L}}), \tag{2}$$

where X_M is the DH-PIM code word.

In DH-PIM with a variable symbol length, an error in one symbol will affect the following symbols, therefore, it is meaningless to access the error performance in terms of the bit error rate. Instead the SER and packet error rate (PER) are adopted to measure the error performance, a characteristic unique to the anisochronous pulse time modulation schemes. Assuming that there is no bandwidth

limitation imposed by the channel, and H_0 and H_1 are equally likely, the probability of symbol and packet errors for the DH-PIM for a LOS link configuration is given by [16]:

$$P_{se} = 0.25\overline{L}^{-1}\left[\left(4\overline{L}-3\alpha\right)Q\left(\frac{\mu k R\overline{P}}{\sqrt{\eta R_b}}\right)+3\alpha Q\left(\frac{\mu(1-k)R\overline{P}}{\sqrt{\eta R_b}}\right)\right]; \quad (3)$$

$$P_{pe} = \frac{N_{Pkt}}{4M}\left[\left(4\overline{L}-3\alpha\right)Q\left(\frac{\mu k R\overline{P}}{\sqrt{\eta R_b}}\right)+3\alpha Q\left(\frac{\mu(1-k)R\overline{P}}{\sqrt{\eta R_b}}\right)\right]; \quad (4)$$

where, $\mu = \sqrt{32M\overline{L}/9\alpha^2}$, $Q(v) = (1/\sqrt{2\pi})\int_{-v}^{\infty}\exp\left(-0.5x^2\right)dx$, k is the threshold level, $\overline{P}$ is the average received optical power, R_b is the input bit rate, N_{pkt} is the packet length in bits and η is the noise power spectral density. Here we use the symbol of L-DH-PIM$_\alpha$ where $L = 2^M$, $\alpha = 2$ for the mathematical derivation and simulation.

3. Convolutional Coded DH-PIM

Convolutional encoding with Viterbi decoding is a forward error correction (FEC) technique appropriate for a channel corrupted mainly by AWGN [18]. A convolutional encoder is a finite state machine with K-shift registers [19] with a predefined connection to n modulo-2 adders. A k-bit input sequence applied to an encoder produces an n-output bits sequence, and hence the code rate r can be approximated as:

$$r = \frac{k}{n} . \quad (5)$$

A convolutional code is parameterised by its constraint length K and r. In this paper we use the symbol (K, n, k) to denote a convolutional encoder. The convolutional encoder can be described by its generator matrix [19]. Here, we use (3, 1, 2) with the function generators g_1 = [111] and g_2 = [101].

On converting a DH-PIM symbol sequence into a CC-DH-PIM symbol, provided the encoder initial state is 'a' (see Fig. 3), the headers will have unique patterns of [11 10 11] or [11 01 01], see Table 1. The encoder is normally at the state 'a' after each symbol since there are two zeros at the end of each DH-PIM symbol except for the symbol with a decimal equivalent of 2^M-1. For symbols with the decimal equivalent of 2^M-1, after a symbol is being generated the encoder will be in the state '*c*' and a different header patterns of [00 10 11] and [00 01 01] will be assigned to the current symbol, as symbols follow either path 3 or 4 in the Trellis diagram in Fig. 3. Thus, CC-DH-PIM symbols with four headers and a limited number of possible paths will have different transfer function and error probability, which is investigated in the following section.

To determine the transfer function, the modified state diagram is illustrated in Fig. 4. In Fig. 4, the exponents *D* and *L* are the Hamming weight of the encoder output corresponding to the branch, and a counting variable to calculate the number of branches in any path, respectively, whereas *I* denotes transition due to the input bit 1. The transfer function of the encoder is given by [19]:

$$T(D,L,I) = D^5L^3I + D^6L^4I^2(1+L) + D^7L^5I^3(1+L)^2 + \ldots \quad (6)$$

The minimum free distance d_{free} for the encoder is 5 increasing with the constraint length as tabulated in [19] for different values of *K* and *r*. Applying the hard-decision Viterbi algorithm [20] to decode $\hat{\boldsymbol{X}}$, the upper bound for the probability of slot error for the coded system P_{se-CC} is given by [19]:

$$P_{se-CC} < \sum_{d=dfree}^{\infty} \beta_d P(d); \quad (7)$$

where β_d is the expansion coefficients of derivative $T(D, I)$, evaluated for $I = 1$, and $P(d)$ is given by:

$$P(d) = \sum_{k=(d+1)/2}^{d} \binom{d}{k} P_{se}{}^{k} (1-P_{se})^{d-k} \qquad \text{if } d \text{ is odd}$$
$$== \sum_{k=d/2+1}^{d} \binom{d}{k} P_{se}{}^{k} (1-P_{se})^{d-k} + \frac{1}{2}\binom{d}{\frac{1}{2}d} P_{se}{}^{d/2} (1-P_{se})^{d/2} \qquad \text{if } d \text{ is even} \tag{8}$$

Instead of using (8), one could use the upper bound for $P(d) < [4P_{se}(1-P_{se})]^{1/2}$, thus (7) becomes as [19]:

$$P_{se-CC} < \left.\frac{\partial T(D,I)}{\partial I}\right|_{I=1, D=\sqrt{4P_{se}(1-P_{se})}} . \tag{9}$$

Using (7) the upper bound for (3, 1, 2) encoder described above is given by:

$$P_{se-CC} < \sum_{d=5}^{\infty} 2^{(d-5)} (d-4) P(d) . \tag{10}$$

Substituting the derivative of (6) into (9) results in:

$$P_{se-CC} << \sum_{d=5}^{\infty} 2^{(d-5)} (d-4) \left(\sqrt{4P_{se}(1-P_{se})}\right)^{d} . \tag{11}$$

Next we consider the transfer function for the coded DH-PIM by studying its trellis diagram outlined in Fig. 4. As can be seen from Fig. 4, there is no path at state 'd' (i.e. no self-loop at state 'd'), therefore the transfer function, as well as the upper bound needs to be modified to the following:

$$T(D,L,I) = \frac{D^5 L^3 I(1+DLI)}{1-DL^2(1+DLI)} \tag{12(a)}$$

$$P_{se-CC} < P(5) + 4P(6) + 9P(7) + 20P(8) \tag{12(b)}$$

4. Results and Discussions

Figure 5 shows the predicted SER performance curves against the electrical signal-to-noise ratio (SNR) for three values of error bounds given by (10), (11) and (12), at a data rate of 1 Mbps and an M of 4. For SER lower than 10^{-6} the upper bound for the CC-DH-PIM and the general error bound for the convolutional coded modulation scheme almost overlap, diverging at lower values of SNR (i.e. higher SER). Since the upper bound for CC-DH-PIM is always less than or equal to the upper bound for its counterparts, then it is expected that it should give similar or even improved performance compared to the other convolutional coded modulation schemes such as OOK even though both could have the same uncoded SER. This is because CC-DH-PIM has fixed header patterns that limit the number of possible paths in the trellis diagram. As a result, the expansion coefficient β_d of (7) is different for the CC-DH-PIM. Comparing the 3rd and 4th terms of (11) and (12), the coefficients are 12 and 32, and 9 and 20, respectively. Although the first two terms are the dominating terms in determining the error bound of lower values of SER, the contribution of other terms can not be neglected for higher values of SER. Hence, the error bounds defined by (11) and (12) will have noticeable differences at low values of SER. In other words, as the number of possible paths decreases, the probability of error decreases. This is because there is only a finite set of paths to choose from, thus making the decoding process much simpler.

For DH-PIM scheme, we used (3, 1, 2) convolutional coding and the Viterbi algorithm with the 'hard' decoding. Assuming an ideal channel and with one-sided power spectral density $\eta = 2q_e I_b$, where q_e is the charge of electron and I_b is set to 200 μA, the proposed CC-DHPIM system was simulated using Matlab. The simulation parameters used and the flow chart for determining the error rates for the CC-DH-PIM are given in Table 2 and Fig. 6, respectively.

Figure 7 provides predicted and simulated results for SER performance for the standard DH-PIM and CC-DH-PIM schemes for $M = 3$ and 4, and a bit rate R_b of 1 Mbps. For $P_{se} < 10^{-2}$ the predicted and simulated curves for the CC-DH-PIM match each other reasonably well. Since it is somewhat difficult to ascertain the exact Hamming distance for the convolutional code in the theoretical analysis, only the upper bound for the error was considered. The simulated SER performance is very close to the upper bound, but is always less than or equal to it. The code gain decreases with the SNR and at very low values of SNR (or SER > 0.1) the code gain is negative. At higher values of SER, introducing coding contributes to more correlated errors from the uncorrelated random errors [21], thus giving rise to additional errors and hence degrading the error performance. A code gain of more than 4 dB is observed for P_{se} of 10^{-4} compared to the standard DH-PIM$_2$ scheme for $M = 3$ and 4, respectively. To achieve a certain SER, the SNR required decreases as M increases. This is expected since the SER of un-coded DH-PIM scheme decreases with M [16]. A difference of almost ~3 dB in the SNR is observed at the SER of 10^{-4} for M of 3 and 4. Similarly in the case of DH-PIM$_1$ scheme a code gain of more than 4 dB is observed at a SER of 10^{-4}.

Detailed comparison of the SER performance of the standard DH-PIM with other modulation schemes is given in [16]. Here we only compare the CC-DH-PIM (upper bound) to the standard DH-PIM and PPM schemes, see Fig. 8. CC-DH-PIM$_1$ offers the best performance compared to the un-coded PPM and DH-PIM, as expected. However, the Trellis coded PPM scheme does outperform all other coded modulation schemes including the CC-DH-PIM. The performance of 16-CC-DH-PIM$_2$ is very close to that of the standard 16-DH-PIM$_1$. The SER of the 16-CC-DH-PIM$_2$ runs almost parallel to the standard 16-DH-PIM$_1$, 16.CC-DH-PIM$_2$ requiring just more than 0.5 dB of SNR to achieve the same SER perfromance. To achieve a SER of 10^{-6}, 16-CC-DH-PIM$_1$ requires ~5 dB lower SNR compared to the standard DH-PIM$_1$, while 16-DH-PIM$_2$ requires about 4 dB more SNR compared to the 16-CC-DH-PIM$_2$.

The performance of the CC-DH-PIM system can be further enhanced by increasing the constraint length, which results in increased code gain but at the cost of increased system complexity. Thus, there exists a trade-off between complexity and performance. Here we have used an encoder/decoder with the constraint length of 7, which are readily available, to asses the performance of the coded DH-PIM system. Simulation results for the SER for the coded 16-DH-PIM for (7, 1, 2) encoder with a generator of (133, 171) in octal number is depicted in Fig. 9. Also shown for comparison are the plots for the standard and 16-CC-DH-PIM cases. The best SER performance is observed for the coded DH-PIM scheme with a constraint length of 7 for SER < 10^{-2}. At very high values of SER (i.e. 0.005), CC-DH-PIM with *K* of 3 and 7 intersect. Thus, indicating that there is no gain in increasing the constraint length. However, at lower values of SER (less than 10^{-3} for any practical systems) there is a marked improvement in the performance when using a longer constraint length. For SER of 10^{-5} the SNR gain of the coded DH-PIM with *K* of 7 are ~2 dB and ~6 dB compared to the coded DH-PIM with *K* of 3 and the standard DH-PIM, respectively for α = 1 and 2. The code gain could be used to increase the link range in indoor optical wireless system.

Conclusions

The paper convolutional coded DH-PIM modulation scheme with the Viterbi 'hard' decoding sachem was considered. Mathematical analysis for the SER with the upper bound was presented. For (3, 1, 2) CC-DH-PIM scheme, predicted results for the slot error rate were compared to the simulation results showing a good match. We have shown that CC-DH-PIM scheme offer a code gain of more than 4 dB at a slot error rate of 10^{-4} compared to standard DH-PIM. We have shown that CC-DH-PIM$_1$ also outperforms the PPM scheme. As expected, the (7, 1, 2) CC-DH-PIM scheme showed improvement over (3, 1, 2) CC-DH-PIM with a code gain of 2 dB at slot error rate of 10^{-5}. However, in CC-DH-PIM the improvement in the error performance is achieved at the cost of reduced transmission throughput compared to the standard DH-PIM scheme.

References

1. Green, R.J., Joshi, H., Higgins, M. D., and Leeson, M. S.: 'Recent developments in indoor optical wireless systems', IET Communications, 2008, 2, (1), pp. 3-10.
2. Smitha, K., Sivabalan, A., and John, J.: 'Estimation of channel impulse response using modified ceiling bounce model in non-directed indoor optical wireless system', Wireless Personal Communications, 2008, 45, (1), pp. 1-10.
3. Al-Ghamdi, A.G., and Elmirghani, J.M.H.: 'Multiple spot diffusing geometries for indoor optical wireless communication system', International Journal of Communication Systems, 2006, 16, (10), pp. 909-922.
4. Arumugam, S., and John, J.: 'Effect of transmitter positions on received power and bandwidth in diffuse indoor optical wireless systems', Optical and Quantum Electronics, 2007, 37, (1), pp. 1-14.
5. Bloom, S., Korevaar, E., Schuster, J., and Willebrand, H.: 'Understanding the performance of free-space optics', Journal of Optical Networking, 2003, 2, (6), pp. 178-200.
6. Kahn, J.M., and Barry, J.R.: 'Wireless infrared communications', Proceedings of IEEE, 1997, 85, (2), pp. 265-298.
7. Heatley, D., Wisely, D.R., and Cochrane, P.: 'Optical wireless: The story so far', IEEE Communications Magazine, 1998, 36, (12), pp. 72-82.
8. Carruthers, J.B.: 'Wireless infrared communications' 2002, Wiley Encyclopaedia of Telecommunications.
9. Giakos, G.C., Panama, N., Sumrain, S., Fraiwan, L., and Kumar, S.: 'A novel multipath light signal dispersion reduction technique based on controlled-polarization optical wireless link setup', IEEE Transaction on Instrumentation and Measurement, 2005, 54, (5), pp. 1950-1956.

10. Carruthers, J.B., and Carroll, S.M.: 'Statistical impulse response models for indoor optical wireless channels', International Journal of Communication Systems, 2005, 18, (3), pp. 267-284.

11. Boucouvalas, A.C.: 'Indoor ambient light noise and its effect on wireless optical links', IEE Proceedings - Optoelectronics, 1996, 143, (6), pp. 334-338.

12. Carruthers, J.B., and Kahn, J.M.: 'Modeling of nondirected wireless Infrared channels', IEEE Transaction on Communication, 1997, 45, (10), pp. 1260-1268.

13. Lee, D.C., and Kahn, J.M.: 'Coding and equalization for PPM on wireless infrared channels', IEEE Transaction on Communication, 1999, 47, (2), pp. 255-260.

14. Shiu, D., and Kahn, J.M.: 'Differential pulse position modulation for power-efficient optical communication', IEEE Transaction on Communication, 1999, 47, (8), pp. 1201-1210.

15. Ghassemlooy, Z., and Hayes, A.R.: 'Digital pulse interval modulation for IR communication systems-a review', International Journal of Communication Systems, 2000, 13, (7-8), pp. 519-536.

16. Aldibbiat, N.M.: 'Optical wireless communication systems employing dual header pulse interval modulation (DH-PIM)', PhD thesis, Sheffield Hallam University, UK, 2001.

17. Sethakaset, U., and Gulliver, T.A.: 'Differential amplitude pulse-position modulation for indoor wireless optical communications', EURASIP Journal on Applied Signal Processing, 2005, 2005, (1), pp. 3-11.

18. Haykin, S.: 'Digital Communications', John Wiley & Sons: New York, 1988.

19. Proakis, J.G.: 'Digital communications', McGraw-Hill, Inc., Fourth ed. 2001.

20. Viterbi, A.J.: 'Error bounds for convolutional codes and an asymptotically optimum decoding algorithm', IEEE Transactions on Information Theory, 1967, 13, (2), pp. 260-269.

21. Wuth, T., Agrell, E., Karlsson, M., and Skold, M.: 'Fiber communications using convolutional coding and bandwidth-efficient modulation', Optics Express, 2006, 14, (2), pp. 542-555.

List of Tables and Figures

Table 1: Symbol structure for OOK, DH-PIM$_2$ and CC- DH-PIM$_2$ preceded by 2^M-1, for $M = 3$.

OOK	DH-PIM$_2$	CC-DH-PIM$_2$
000	**100**	**11 10 11**
001	**100** 0	**11 10 11** 00
010	**100** 00	**11 10 11** 00 00
011	**100** 000	**11 10 11** 00 00 00
100	**110** 000	**11 01 01** 11 00 00
101	**110** 00	**11 01 01** 11 00
110	**110** 0	**11 01 01** 11 00
111	**110**	**11 01 01**

Table 2: The simulation parameters for the system described in Fig. 1

Parameters	**Values**
M	3 an 4
α	2
Detector responsivity R	1 A/W
Background noise current I_b	200 μA
Bit rate R_b	1 Mbps
Threshold level k	0.5
Pulse duty cycle	100 %
Number of DH-PIM symbols	10^5

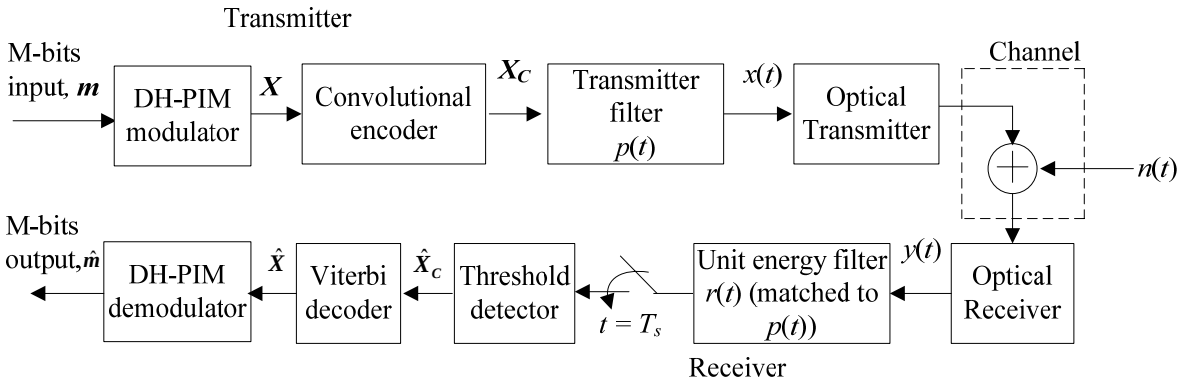

Fig. 1: A block diagram of CC-DH-PIM scheme.

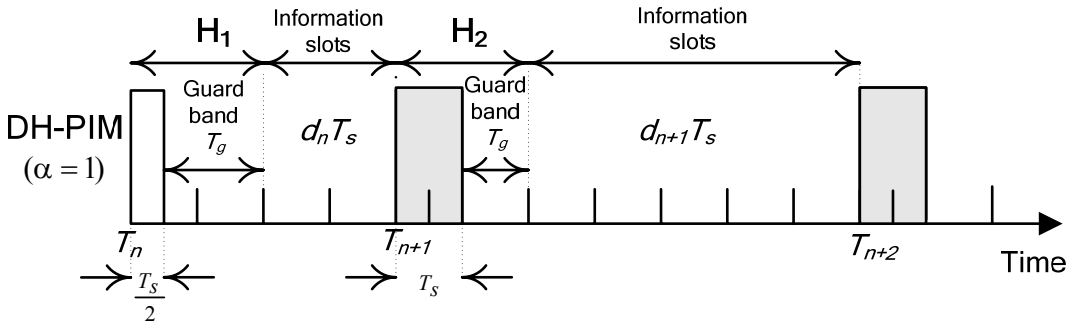

Fig. 2: DH-PIM symbol structure for $\alpha = 1$ and $M = 4$.

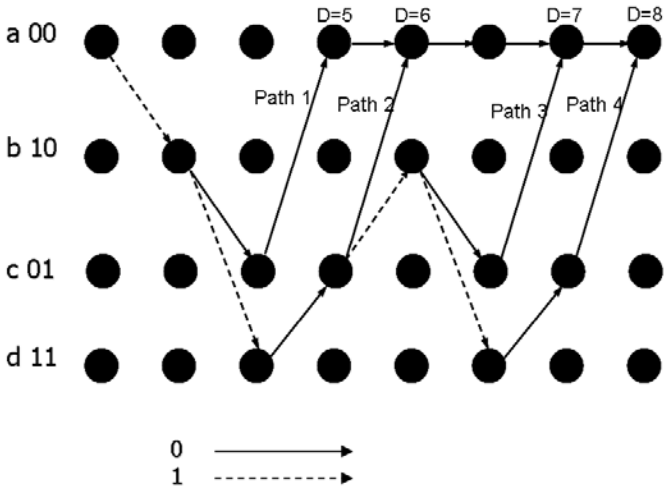

Fig. 3: Trellis diagram of CC-DH-PIM$_2$.

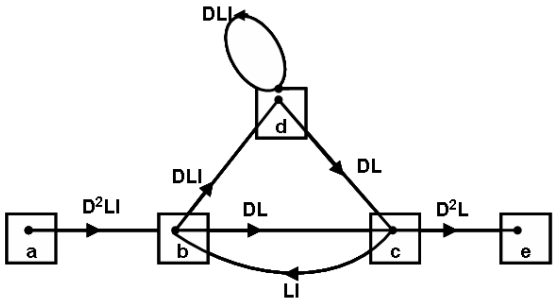

Fig. 4: Modified state diagram for general convolutional encoder.

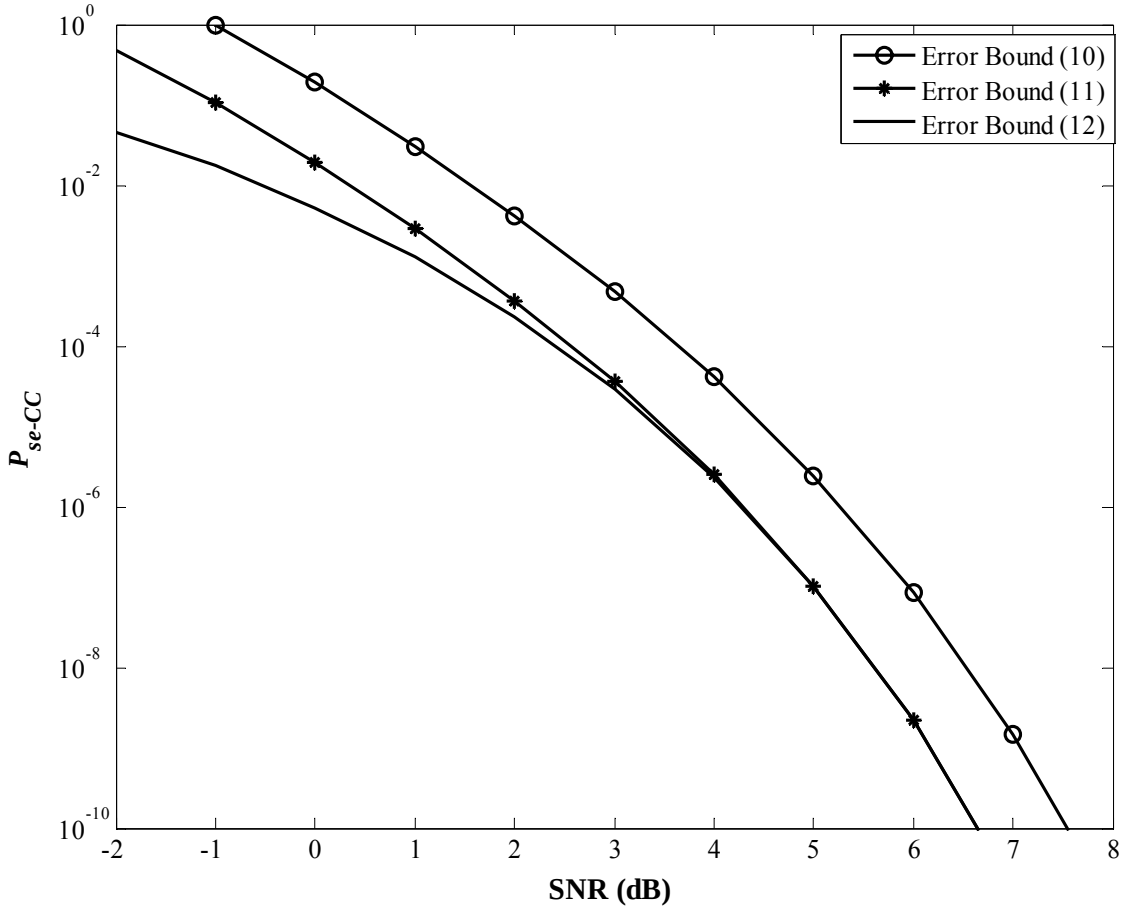

Fig. 5: The SER against SNR for different error bound for CC-DH-PIM$_2$.

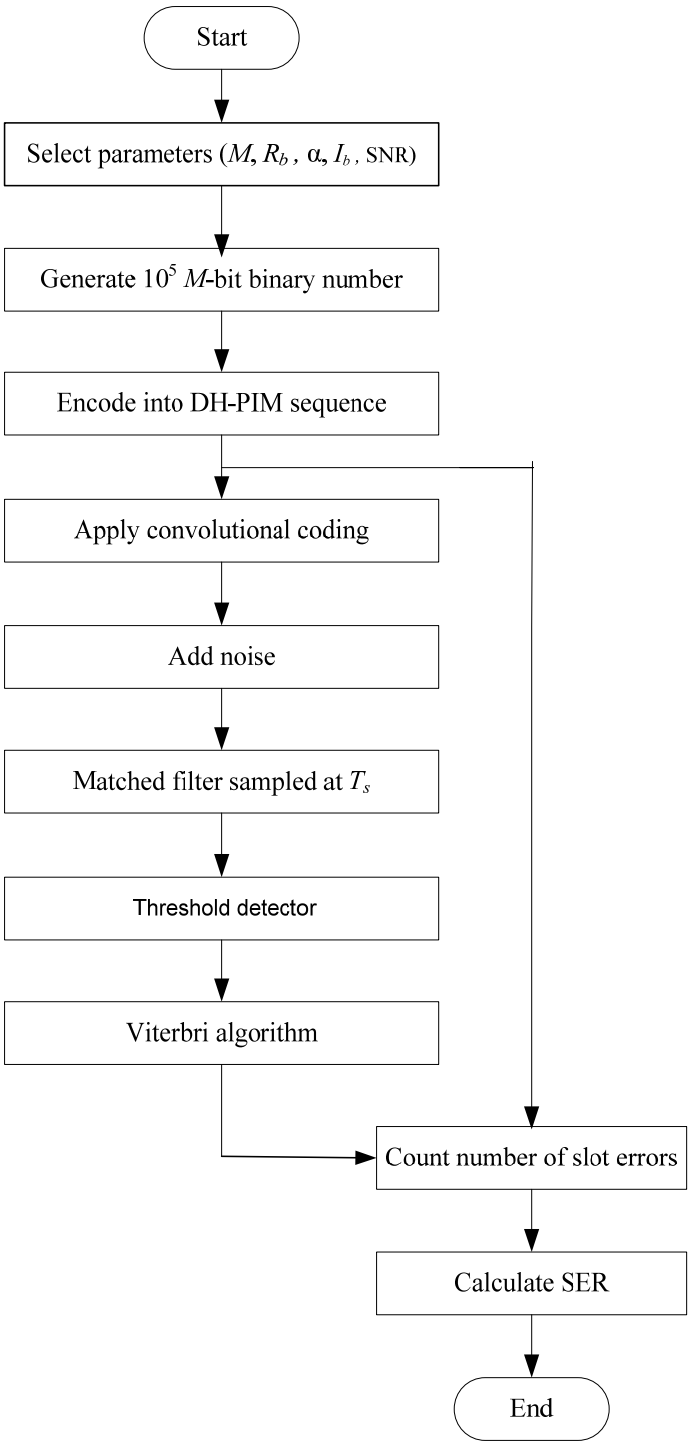

Fig. 6: A flow chart diagram for determining the SER of the CC-DH-PIM shown in Fig.1.

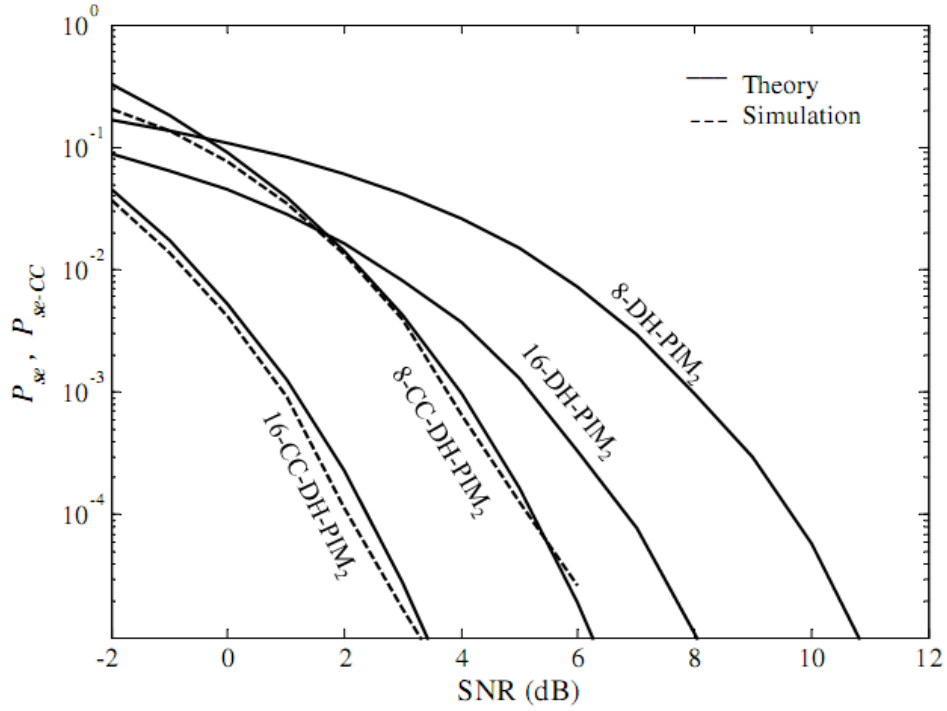

(a)

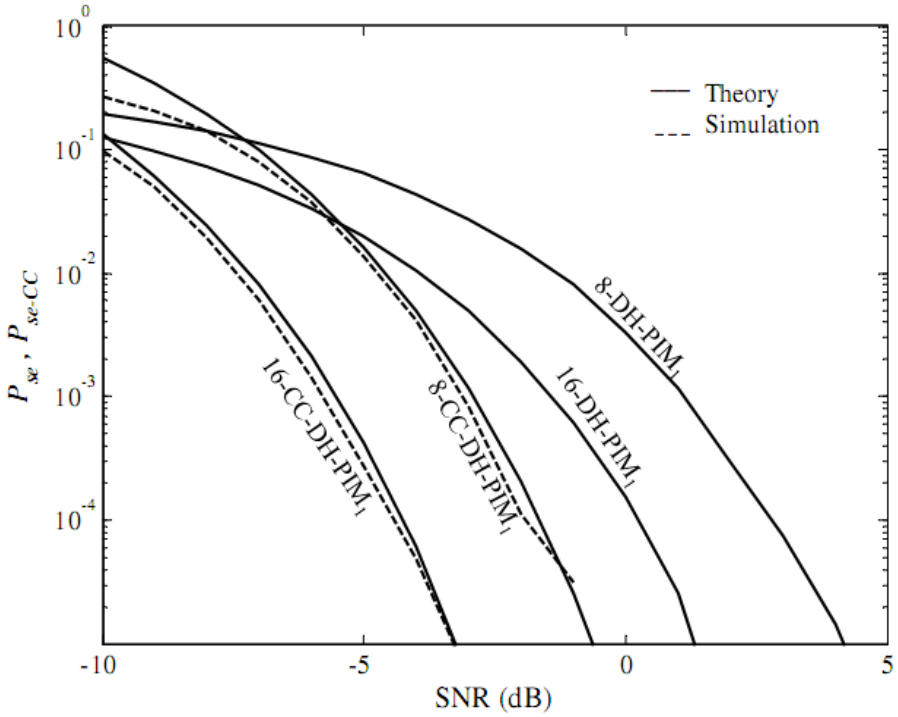

(b)

Fig. 7: The SER versus the SNR for M = 3 and 4 and R_b = 1 Mbps: (a) standard DH-PIM$_2$ and CC-DH-PIM$_2$, (b) standard DH-PIM$_1$ and CC-DH-PIM$_1$.

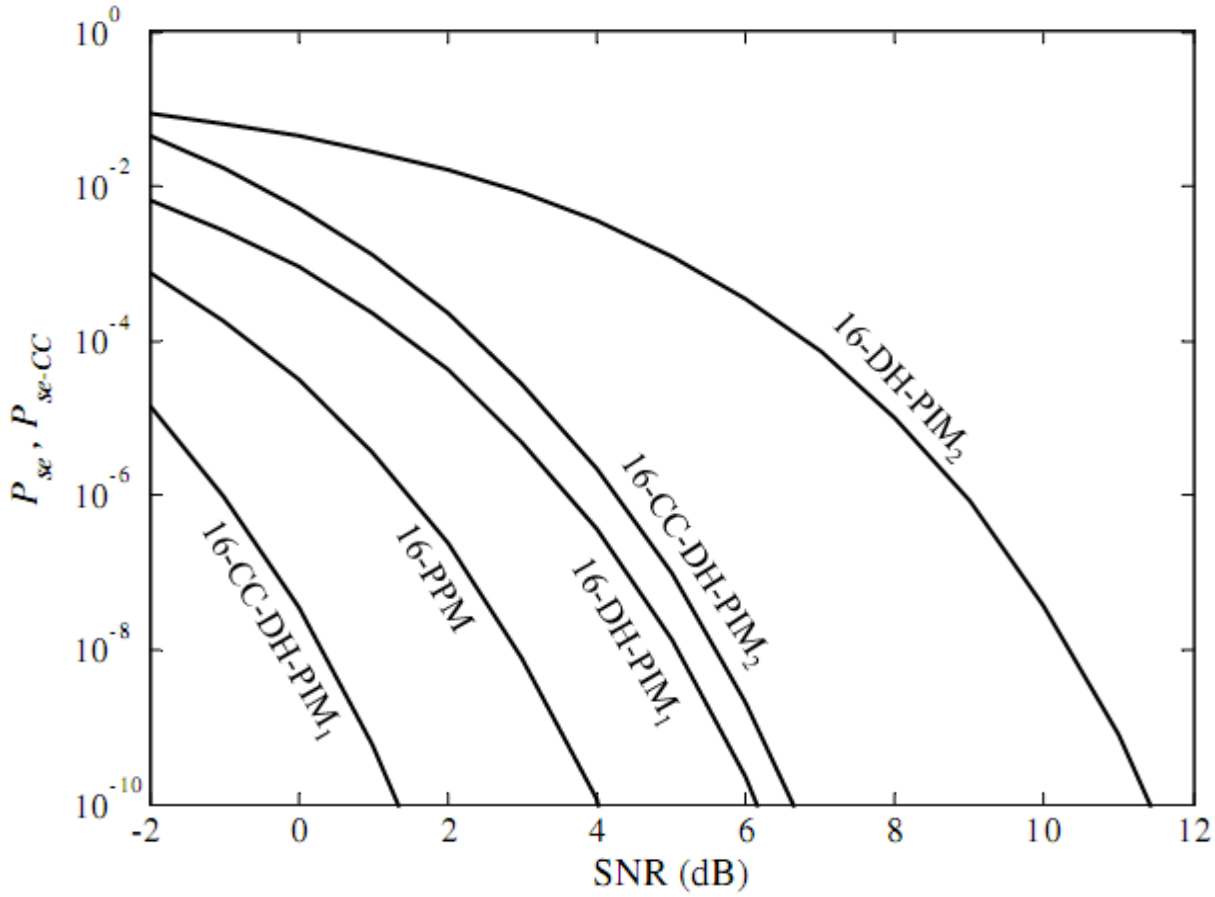

Fig. 8: Comparison of slot error rate for different modulation techniques.

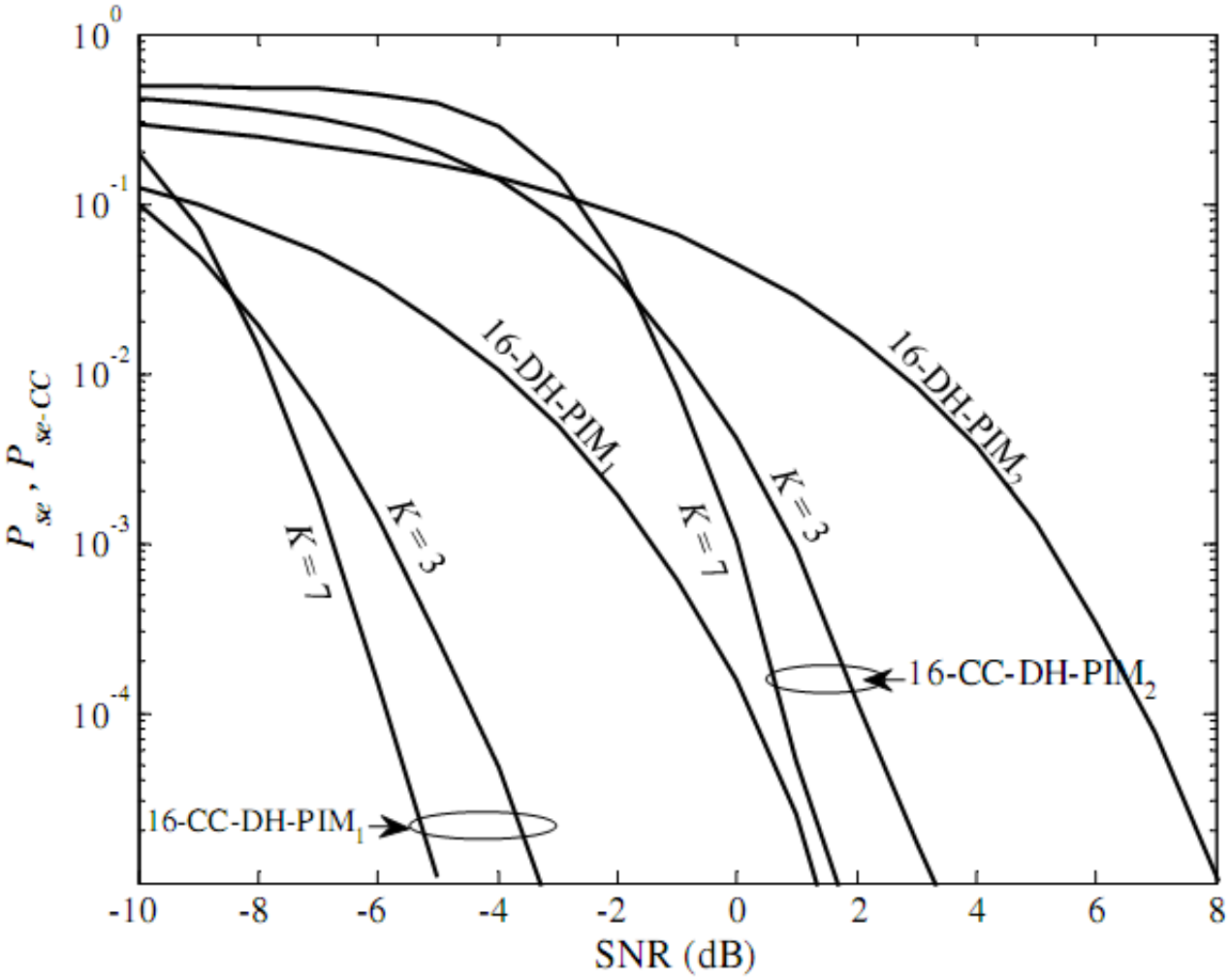

Fig. 9: The SER against SNR for code and un-coded 16-DH-PIM for constraint length of 3 and 7.